



ELSEVIER

Journal of Alloys and Compounds 340 (2002) 173–179

Journal of  
ALLOYS  
AND COMPOUNDS

www.elsevier.com/locate/jallcom

# Fabrication and electrical and thermal properties of $Ti_2InC$ , $Hf_2InC$ and $(Ti,Hf)_2InC$

M.W. Barsoum<sup>a,\*</sup>, J. Golczewski<sup>b</sup>, H.J. Seifert<sup>b</sup>, F. Aldinger<sup>b</sup><sup>a</sup>Department of Materials Engineering, LeBow Engineering Center 27-445, Drexel University, Philadelphia, PA 19104-2875, USA<sup>b</sup>Max-Planck-Institut für Metallforschung, Stuttgart, Germany

Received 12 December 2001; accepted 8 January 2002

## Abstract

In this paper we report on the characterization of predominantly single phase, fully dense  $Ti_2InC$  ( $Ti_{1.96}InC_{1.15}$ ),  $Hf_2InC$  ( $Hf_{1.94}InC_{1.26}$ ) and  $(Ti,Hf)_2InC$  ( $(Ti_{0.47},Hf_{0.56})_2InC_{1.26}$ ) samples produced by reactive hot isostatic pressing of the elemental powders. The  $a$  and  $c$  lattice parameters in nm, were, respectively: 0.3134; 1.4077 for  $Ti_2InC$ ; 0.322, 1.443 for  $(Ti,Hf)_2InC$ ; and 0.331 and 1.472 for  $Hf_2InC$ . The heat capacities, thermal expansion coefficients, thermal and electrical conductivities were measured as a function of temperature. These ternaries are good electrical conductors with a resistivity that increases linearly with increasing temperatures. At 0.28  $\mu\Omega$  m, the room temperature resistivity of  $(Ti,Hf)_2InC$  is higher than the end members ( $\sim 0.2$   $\mu\Omega$  m), indicating a solid solution scattering effect. In the 300 to 1273 K temperature range the thermal expansion coefficients are:  $7.6 \times 10^{-6}$   $K^{-1}$  for  $Hf_2InC$ ,  $9.5 \times 10^{-6}$   $K^{-1}$  for  $Ti_2InC$ , and  $8.6 \times 10^{-6}$   $K^{-1}$  for  $(Ti,Hf)_2InC$ . They are all good conductors of heat (20 to 26 W/m K) with the electronic component of conductivity dominating at all temperatures. Extended exposure of  $Ti_2InC$  to vacuum ( $\sim 10^{-4}$  atm) at  $\sim 800$  °C, results in the selective sublimation of In, and the conversion of  $Ti_2InC$  to  $TiC_x$ . © 2002 Elsevier Science B.V. All rights reserved.

**Keywords:** Intermetallics; Synthesis; Crystal structure; Electrical transport; X-ray diffraction

## 1. Introduction

This paper is a continuation of our work on the syntheses, fabrication and characterization of the so-called MAX phases [1–15]. These compounds, with the general formula  $M_{n+1}AX_n$  where  $n=1$  to 3, M is an early transition metal, A is an A-group (mostly IIIA and IVA) element, and X is either C and/or N are structurally related. These layered hexagonal phases—space group  $D_{6h}^4$ ,  $P6_3/mmc$ —with two formula units per unit cell, have been shown to exhibit an unusual and unique combination of properties [1–15].

There are several reasons these solids represent a new class of solids. They are the only polycrystalline solids in which single grains can deform by a combination of slip, kink band formation and delaminations [1,5,6]. The extent by which grains can delaminate and deform at room temperature is unique. Basal plane dislocations, and only basal plane dislocations, are mobile and multiply at room

temperatures [5,6]. Some of them are elastically quite stiff (the stiffness of  $Ti_3SiC_2$ —320 GPa—is almost three times that of Ti metal, with the *same* density) but are most readily machinable using manual hack saws or regular high speed tool steels with no lubrication or cooling required. They are also excellent conductors of electricity and heat [1,8–10,12] ( $Ti_3SiC_2$  has higher electrical and thermal conductivities than Ti metal). With Vickers hardness values in the range 2–5 GPa, these compounds are soft compared to other early transition metal carbides and nitrides. They are also exceptionally thermal shock-resistant and damage-tolerant for their stiffness. The latter two characteristics are traceable to the presence of an active slip system.

This paper deals with the phases  $Ti_2InC$ ,  $Hf_2InC$  and  $(Ti,Hf)_2InC$  with a Ti/Hf ratio of 1. In the early 1960s, the end members were first synthesized in powder form by Jeitschko et al. [16], who determined their structure and lattice parameters. These phases have never been characterized before, and as such could possess unique electrical, magnetic, thermal or catalytic properties for potential use in many applications. For example, it has recently been shown that the thermoelectric power of  $Ti_3SiC_2$  is negligible at least over the 300–850 K temperature range

\*Corresponding author. Tel.: +1-215-895-2338; fax: +1-215-815-6760.

E-mail address: michel.w.barsoum@drexel.edu (M.W. Barsoum).

[7,11]. Furthermore, the basal planes of  $\text{Ti}_3\text{SiC}_2$  have been shown to possess very low friction coefficients [15]. Low friction, good wear resistance and good electrical conductivity is a useful combination of properties that can potentially be used in rotating electrical contacts such as motor brushes. These could also potentially be used as diffusion barriers, or heat sinks in Si-based devices.

This paper is the first report on the synthesis and characterization of predominantly single phase, dense samples of  $\text{Ti}_2\text{InC}$ ,  $\text{Hf}_2\text{InC}$  and  $(\text{Ti,Hf})_2\text{InC}$ . The heat capacity, thermal expansion, thermal and electrical conductivities of these compounds were measured as a function of temperature.

## 2. Experimental details

Elemental Hf (99.6% pure excluding 2–3.5% Zr), Ti (99%), In (99.99%) and graphite (99.9995%)–325 mesh powders were used. The purities, based on metal basis alone, are those specified by the supplier (Alpha Aesar, Karlsruhe, Germany). The powders were weighed in the proper stoichiometric ratios, mixed and cold isostatically pressed using a pressure of 630 MPa. The cylindrical pellets were sealed in borosilicate glass tubes under vacuum, placed in a hot isostatic press, HIP, and heated at  $20^\circ\text{C}/\text{min}$  to  $700^\circ\text{C}$ , held at that temperature for 30 min, before Ar was introduced in the chamber. The HIP was then heated at the same rate to  $1300^\circ\text{C}$ , where it was held for 7 h before cooling. The pressure at  $1300^\circ\text{C}$  was  $\sim 50$  MPa.

The glass was mechanically removed, and the samples were mounted and polished down to  $1\ \mu\text{m}$  diamond for microstructural evaluation in a scanning electron microscope, SEM. The chemical composition was measured by electron probe X-ray microanalysis (EPMA) which was performed on a Cameca SX100 (Paris, France). Measurements were carried out using an accelerating voltage of 15 kV, and a probe current of 20 nA for all but the Hf. For the Hf, the accelerating voltage was 20 kV with the same current. The following standards were used for the quantitative analysis: pure Ti for Ti,  $\text{Fe}_3\text{C}$  for C, Hf for Hf and InP for In. The  $\text{K}\alpha$  lines were used for the first two and the  $\text{L}\alpha$  lines for the last two.

The lattice parameters were measured from X-ray diffraction, XRD, patterns using a diffractometer (D5000, Siemens/Bruker AXS, Karlsruhe, Germany) with a position-sensitive detector and Ni-filtered  $\text{Cu}\ \text{K}\alpha_1$  radiation. The step size was  $0.008^\circ$  and the step time was 1 s. The powdered samples were obtained by drilling into the center of the samples; Si powder was used as an internal standard. The intensity ratios were calculated from the areas under the peaks and no attempt was made to reduce preferred orientations. The density,  $\delta$ , was measured by Archimedes' principle in water.

The heat capacities,  $c_p$ , were measured using a differen-

tial scanning calorimeter, DSC, (Netzsch, 404C, Selb, Germany). The DSC was calibrated using a sapphire crystal; the calibration and all measurements were carried out under Ar at a heating rate of 10 K/min. The samples were cylindrical (5 mm in diameter and  $\sim 1$  mm thick). The thermal conductivity,  $D$ , was measured using a laser-flash technique. A flat cylindrical (11 mm diameter, 1 mm thick) sample is placed in a vacuum furnace ( $10^{-4}$  atm) and heated to a predetermined temperature, at which time, the front surface is pulsed, for 1 ms, with a 40-J pulse of an Nd:YAG laser. The increase in temperature on the rear surface was monitored with a pyrometer and the temperature versus time curve was digitized and analyzed to estimate the half-time lag,  $t_{1/2}$ , between the initial and the stable final temperatures. The  $D$  values are calculated assuming,  $D = 0.1339d^2/t_{1/2}$ . The  $D$ s are then converted to thermal conductivities,  $k_{\text{tot}}$ , using the relationship:  $k_{\text{tot}} = c_p D \delta$ .

The electrical resistances were measured using a 4-probe technique at 290 K, 273.15 K, 77 K and 4.2 K.

## 3. Results and discussion

### 3.1. Sample characterization

According to the XRD patterns (Fig. 1) the samples were predominantly single phase. The lattice parameters of the end members are in good agreement with those measured by Jeitschko et al. [16] (see Table 1). As expected, the lattice parameters of the solid solution are in

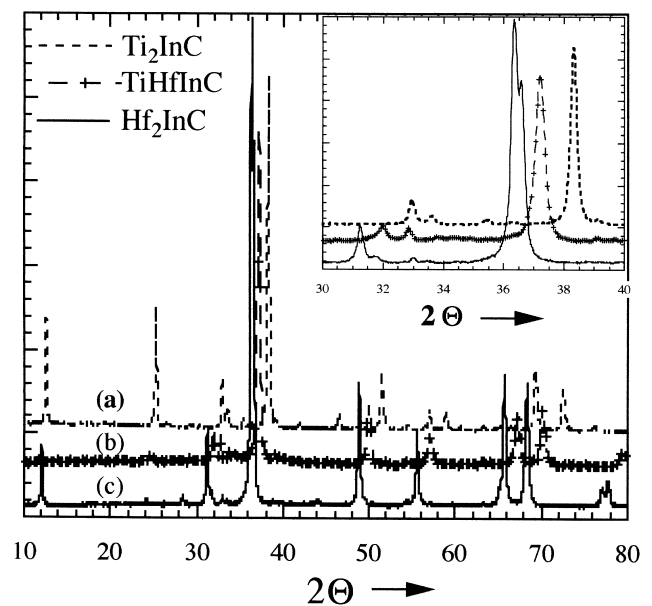


Fig. 1. XRD patterns of (a)  $\text{Ti}_2\text{InC}$ , (b)  $(\text{Ti,Hf})_2\text{InC}$ , and (c)  $\text{Hf}_2\text{InC}$ . Inset shows details of area around  $2\theta = 35^\circ$ , which clearly show that the diffraction lines of the solid solution lie in between those of the end members.

Table 1

Summary of properties of  $M_2\text{InC}$  phases measured in this work. Also included are the lattice parameters measured in this work and those of Jeitschko et al. [16]

Property	$\text{Ti}_2\text{InC}$	$(\text{Ti,Hf})_2\text{InC}$	$\text{Hf}_2\text{InC}$	Comments
Measured density ( $\text{Mg}/\text{m}^3$ )	6.3	8.74	11.24	
Theoretical density ( $\text{Mg}/\text{m}^3$ )	6.2	9.03	11.57	
Lattice parameters ( $\text{\AA}$ )				
$a$	3.134	3.221	3.309	This work
$c$	14.077	14.429	14.723	This work
$a$	3.13	–	3.30	Ref. [16]
$c$	14.06	–	14.73	Ref. [16]
Mol. wt. ( $\text{g}/\text{mol}$ )	222.62	353.21	483.80	
Molar volume ( $\text{g}/\text{cm}^3$ )	35.9	40.6	41.81	
Unit cell volume ( $\text{m}^3$ )	$1.2 \times 10^{-28}$	$1.3 \times 10^{-28}$	$1.39 \times 10^{-28}$	
$\rho_0$ ( $\mu\Omega \text{ m}$ )	0.20	0.28	0.19	
$\alpha$ ( $\text{K}^{-1}$ )	0.0030	0.0025	0.0033	70–300 K
TCE ( $\text{K}^{-1}$ )	$9.5 \times 10^{-6}$	$8.65 \times 10^{-6}$	$7.6 \times 10^{-6}$	RT–1273 K
$k_{\text{tot}}$ ( $\text{W}/\text{m K}$ )	$\sim 26.6 \pm 0.4$	$18 + 0.004T$	$26.5 \pm 1$	450–1350 K

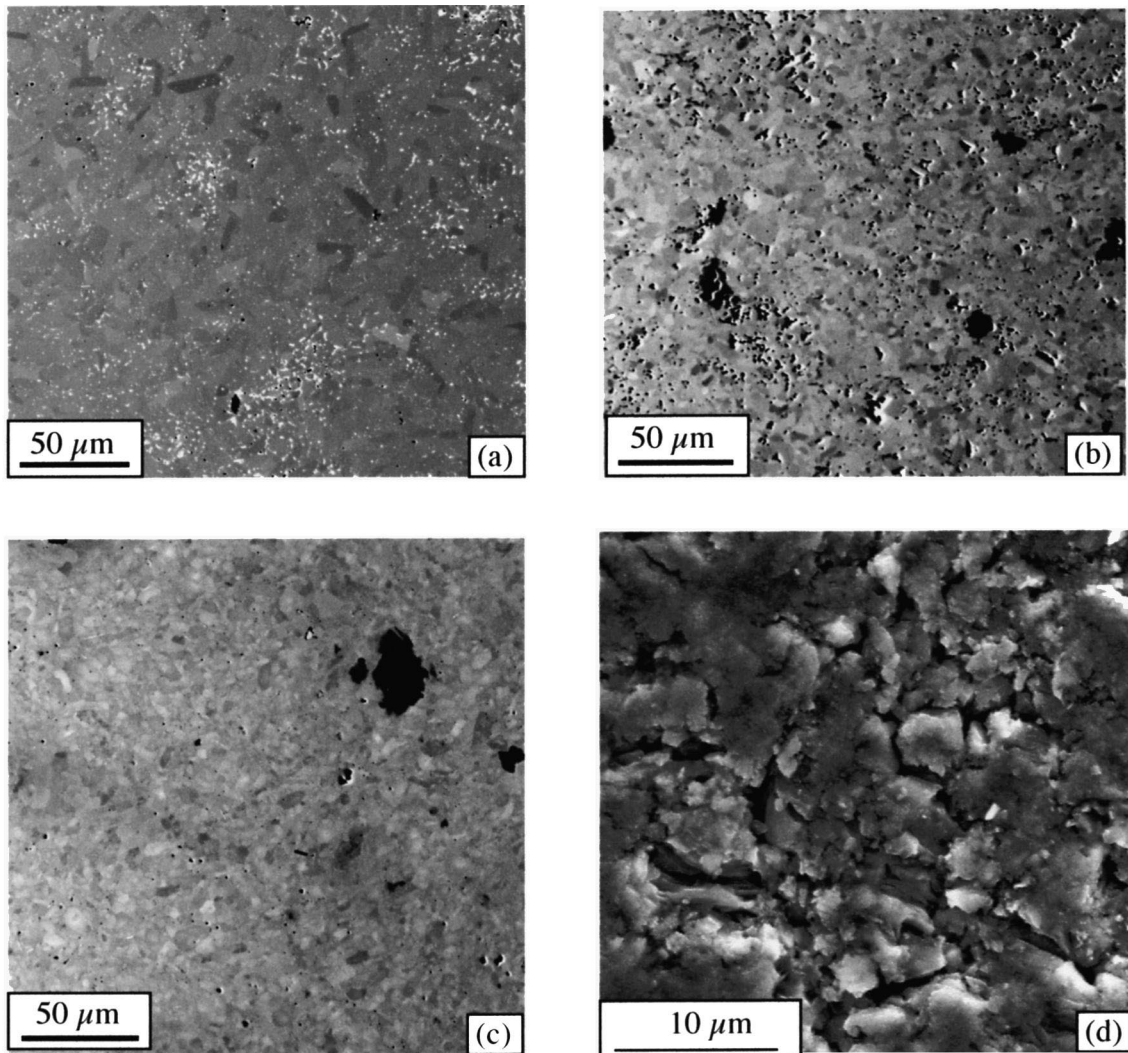


Fig. 2. Backscattered SEM micrographs of (a)  $\text{Ti}_2\text{InC}$ , (b)  $\text{Hf}_2\text{InC}$ , (c)  $(\text{Ti,Hf})_2\text{InC}$ , (d)  $\text{Ti}_2\text{InC}$  sample after 2-h hold in vacuum at  $900^\circ\text{C}$ . Dark areas in (b) and (c) are  $\text{HfC}$  and  $\text{HfO}_2$ , respectively.

between those of the end members. The XRD results for the three compounds are summarized in Appendix A, and again compared to the available data [16]. Based on these results it is fair to assume that a complete solid solubility occurs between  $\text{Ti}_2\text{InC}$  and  $\text{Hf}_2\text{InC}$ .

A typical backscattered SEM micrograph of the  $\text{Ti}_2\text{InC}$  composition is shown in Fig. 2a. The sample is fully dense and comprised of two phases; a gray matrix phase,  $\text{Ti}_2\text{InC}$ , and a white discrete phase, which is In. The volume fraction of the latter is  $\sim 5$  vol.%. According to EPMA of the matrix phase, atomic ratios in % of Ti:In:C are  $47.6(\pm 0.2):24.3(\pm 0.06):28.0(\pm 0.1)$ . The numbers in brackets denote the standard deviations. If one assumes the In sites to be fully occupied, the resulting chemistry would be  $\text{Ti}_{1.96}\text{InC}_{1.15}$ . The grains vary in size from 8 to 50  $\mu\text{m}$ . They are plate-like with aspect ratios of  $\sim 3$ . The measured density ( $6.3 \text{ Mg/m}^3$ ) is in very good agreement with the theoretical density calculated from the lattice parameters (Table 1).

Typical backscattered SEM micrographs of the  $\text{Hf}_2\text{InC}$  and  $(\text{Ti,Hf})_2\text{InC}$  compositions are shown in Fig. 2b and c, respectively. Here again the samples are almost fully dense and predominantly single phase. In both cases, the measured densities are in excellent agreement with those calculated from the lattice parameters (Table 1). The major impurity phase in  $\text{Hf}_2\text{InC}$  is  $\text{HfC}$  (dark phase in Fig. 2b); in  $(\text{Ti,Hf})_2\text{InC}$  it is  $\text{HfO}_2$  (dark phase in Fig. 2c). Their volume fractions are quite low, however. The Hf:In:C ratio in  $\text{Hf}_2\text{InC}$  (dark phase in Fig. 2c) is  $46.1(\pm 0.75):23.8(\pm 0.5):30.0(\pm 1.2)$ . Similarly, the Ti:Hf:In:C ratio in the solid solution is:  $21.8(\pm 0.7):25.5(\pm 0.5):23.1(\pm 0.05):29.4(\pm 0.1)$ . Once again assuming the In sublattice to be fully occupied, one obtains:  $\text{Hf}_{1.94}\text{InC}_{1.26}$  and  $(\text{Ti}_{0.47},\text{Hf}_{0.56})_2\text{InC}_{1.26}$ , for the Hf-211 phase and solid solution, respectively.

### 3.2. Electrical conductivity

Like all the MAX phases characterized to date, the resistivities,  $\rho$ , of the ones studied here fall linearly with decreasing temperature (Fig. 3). Hence  $\rho$  can be represented by:

$$\rho = \rho_0[1 + \alpha(T - 300)] \text{ for } T > 70 \text{ K}$$

where  $\rho_0$ ,  $\alpha$  and  $T$  are, respectively, the resistivity at 300 K, the temperature coefficient of resistivity and the temperature in Kelvin. The values of  $\rho_0$  and  $\alpha$  obtained from a least squares fit of the data are listed in Table 1. The most conductive is  $\text{Ti}_2\text{InC}$ , followed by  $\text{Hf}_2\text{InC}$ , with the least conductive being the solid solution. The residual resistivity of the  $\text{Hf}_2\text{InC}$  is smaller than  $\text{Ti}_2\text{InC}$ , indicating that it may be less defective; the difference is small, however.

Given that the residual resistivity of the solid solution is significantly higher than the end members (Fig. 3) it is fair to conclude that solid solution scattering is occurring in

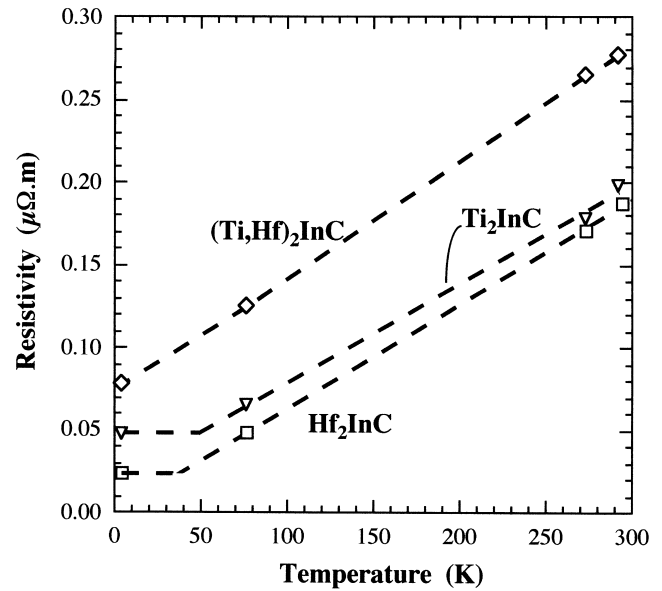


Fig. 3. Temperature dependence of resistivity. The resistivity of the solid solution is higher than the end members.

this system. The same phenomenon occurs in the Ti–Nb–Al–C system where the resistivity of  $(\text{Ti,Nb})_2\text{AlC}$  is significantly higher than its end members,  $\text{Ti}_2\text{AlC}$  and  $\text{Nb}_2\text{AlC}$  [12]. It is worth noting that a similar effect was not observed in  $\text{Ti}_2\text{AlC}_{0.5}\text{N}_{0.5}$  vis-à-vis its end members,  $\text{Ti}_2\text{AlC}$  and  $\text{Ti}_2\text{AlN}$  [13].

### 3.3. Thermal properties

The functional dependence of the thermal strains on temperature are shown in Fig. 4. Least squares fits of the results—on both heating and cooling and over the entire

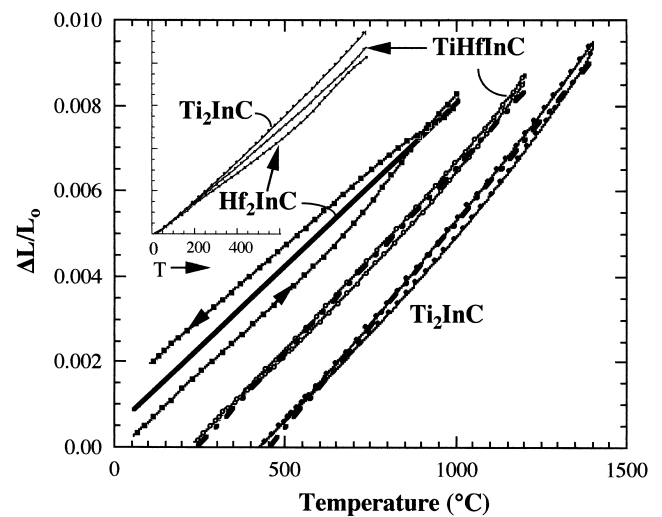


Fig. 4. Bulk dilatometric thermal expansions. The curves are shifted to the right by  $200^\circ$  for the sake of clarity. Inset clearly shows that the  $\text{Ti}_2\text{InC}$  expands at a higher rate than the  $\text{Hf}_2\text{InC}$ , with the solid solution in between.

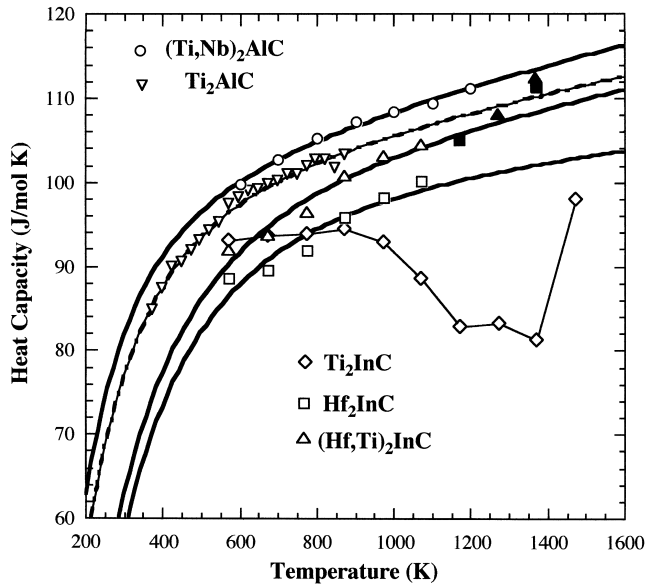


Fig. 5. Temperature dependence of heat capacity for the In-containing phases measured here. Also included are the results for  $\text{Ti}_2\text{AlC}$  and  $(\text{Ti,Nb})_2\text{AlC}$  [12]. The solid lines represent the least squares fits of the data points to the Debye solid.

range measured—yield a mean thermal coefficient of expansion, TCE, of  $9.5 \times 10^{-6} \text{ K}^{-1}$  and  $8.65 \times 10^{-6} \text{ K}^{-1}$ , for  $\text{Ti}_2\text{InC}$  and  $(\text{Ti,Hf})_2\text{InC}$ , respectively. The fits, depicted by dark dotted straight lines, have  $R^2$  values  $>0.99$ . For reasons that are not entirely clear,  $\text{Hf}_2\text{InC}$  exhibits a hysteresis upon cooling. Least squares fits of the heating and cooling portions yields  $8.37 \times 10^{-6} \text{ K}^{-1}$  and  $6.8 \times 10^{-6} \text{ K}^{-1}$ , respectively, for an average of  $7.6 \times 10^{-6} \text{ K}^{-1}$ , which is plotted in Fig. 4 as a solid black line. It is interesting to note that, the two other Hf-containing MAX phases explored to date, viz.  $\text{Hf}_2\text{SnC}$  and  $\text{Hf}_2\text{PbC}$  [14], also exhibit marked hysteresis upon heating and cooling.

We have previously shown a correlation between the TCEs of the MAX phases and their near-stoichiometric MX counterparts [14]. The results obtained here are in agreement with this general principle. The TCE of  $\text{Ti}_2\text{InC}$  is presumably higher than that of  $\text{Hf}_2\text{InC}$  because the TCE of near-stoichiometric  $\text{TiC}$  ( $7.4 \times 10^{-6} \text{ K}^{-1}$  [17]) is higher than that of  $\text{HfC}$  ( $6.6 \times 10^{-6} \text{ K}^{-1}$  [17]). It thus appears that forming solid solutions on the M-sites results in TCE changes that are reasonably well represented by the rule of mixtures. The same is true for the Ti–Nb–Al–C system [12]. This is in contrast to the Ti–Al–C–N system, where the order of the TCEs is:  $\text{Ti}_2\text{AlC}_{0.5}\text{N}_{0.5} > \text{Ti}_2\text{AlC} \sim \text{Ti}_2\text{AlN}$ ,

i.e. the solid solution results in a destabilization of the structure [13].

The effect of temperature on the heat capacities,  $c_p$ s, of the In compounds is shown in Fig. 5. Also included for comparison are the results for  $(\text{Ti,Nb})_2\text{AlC}$  and  $\text{Ti}_2\text{AlC}$ . The  $c_p$ s of  $\text{Hf}_2\text{InC}$  and the solid solution increase gradually with increasing temperatures starting at  $\sim 500 \text{ K}$  up to  $1100 \text{ K}$ , after which the increases are more rapid. Since such increases cannot be intrinsic to the samples, they are most likely due to sample oxidation due to the presence of residual oxygen in the Ar gas used during the measurements. The two heavy dark lines through the data points represent a least squares Debye model fit of the results. Excluded from the fits are the data points represented by solid triangles and squares (top right in Fig. 5). The Debye fits were in turn fit to a third degree polynomial (not shown), the coefficients of which are listed in Table 2 and are only valid in the 400 to 1450 K range.

In the case of  $\text{Ti}_2\text{InC}$  (open diamonds in Fig. 5),  $c_p$  appears to first increase slightly, drop at  $\sim 900 \text{ K}$ , plateau at a minimum around  $1300 \text{ K}$ , before increasing again. Such complex behavior is not expected from a single phase solid that does not go through phase transitions. The increase at higher temperatures is most likely due to oxidation; the drop in  $c_p$ , on the other hand, must be related to the loss of In from the sample (see below). Such a loss would be endothermic and thus appear as a trough in Fig. 5, as observed. Given that the results shown cannot be used to determine  $c_p$  of  $\text{Ti}_2\text{InC}$  or its temperature dependence, the assumption was made that  $c_p$  of the latter was identical to that of  $(\text{Ti,Hf})_2\text{InC}$ . It is important to note that this problem was encountered only during the  $c_p$  measurements because of the small samples we had to use. It is hereby acknowledged that the heat capacity measurements should be repeated with larger samples where the surface to volume ratio is reduced.

The effect of temperature on the thermal conductivity,  $k_{\text{tot}}$ , is shown in Fig. 6. The thermal conductivities of the end members are, given the error bars, almost identical at  $\sim 26.5 \text{ W/m K}$ ; those of the solid solution are lower. A least squares fit of the solid solution results yields the relationship listed in Table 1 (last row). Note that if the phonon contribution,  $k_{\text{ph}}$  to the total thermal conductivity is negligible and/or temperature-independent, mathematically  $dk_{\text{tot}}/dT$  will have the same sign as the intercept of  $\rho$  with the y-axis. Since for the solid solution the intercept is positive (Fig. 3),  $dk_{\text{tot}}/dT$  is also positive (Fig. 6).

In previous work, the Wiedemann–Franz Law ( $k_e =$

Table 2

Coefficients of third order polynomial of  $c_p$  ( $= A + BT + CT^2 + DT^3$ ) that was fit to the Debye model. Values are in J/mol K

	A	B	C	D	
$\text{Hf}_2\text{InC}$	26.0	0.17	$-1.37 \times 10^{-4}$	$3.82 \times 10^{-8}$	Only valid in the 400 to 1450 K range
$(\text{Ti,Hf})_2\text{InC}$	35.2	0.15	$-1.2 \times 10^{-4}$	$3.35 \times 10^{-8}$	
$\text{Ti}_2\text{InC}$	Same as $(\text{Ti,Hf})_2\text{InC}$				

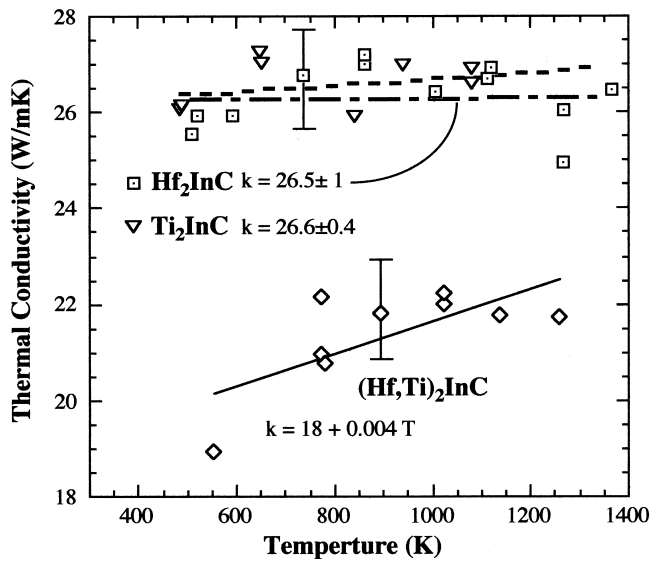


Fig. 6. Temperature dependence of thermal conductivity. Typical error bars are shown in figure.

$L_o T / \rho$ , where  $L_o = 2.45 \times 10^{-8} \text{ W } \Omega / \text{K}^2$ ) was used to estimate the electronic contribution,  $k_e$ , to  $k_{\text{tot}}$  [1,8–10,12]. In some cases, the law was applicable without modifications [8,9]; in others the nonsensical result that  $k_e > k_{\text{tot}}$  was obtained, which by necessity implies that  $L_o$  has to be  $< 2.45 \times 10^{-8} \text{ W } \Omega / \text{K}^2$  [10,12]. The same applies here; in all cases  $k_e > k_{\text{tot}}$ . From this it is concluded that in the compounds studied herein the heat is predominantly carried by delocalized electrons and  $L_o < 2.45 \times 10^{-8} \text{ W } \Omega / \text{K}^2$ . This is not surprising since, with a few notable exceptions, the majority of the heat in the MAX phases is carried by electronic defects [1].

During the thermal diffusivity measurements, it was noted that a thin silver mirror formed on the glass windows capping the furnace tube. The film formed at higher temperatures and, while occurring for all three compounds, was most severe for the  $\text{Ti}_2\text{InC}$  samples. In some cases, the film became so thick that it interfered with the signal and rendered the measurements meaningless. Since this behavior was only observed with In-containing MAX

Table A.1

Summary of XRD results for  $\text{Hf}_2\text{InC}$ . The calculated  $d$ s are based on  $c$  and  $a$  values of 14.723 Å and 3.309 Å, respectively

$h k l$	$2\theta$ , measured	Observed $d$ , (Å)	Calculated $d$ , (Å)	$I/I_{\text{max}}$ measured	$I/I_{\text{max}}$ calculated [11]
0 0 2	12.054	7.3362	7.361	15.6	5.7
0 0 4	24.202	3.6744	3.68	19.2	1.4
1 0 0	31.176	2.8666	2.8656	25.3	23.2
1 0 3	36.295	2.4721	2.4753	100	100
0 0 6	36.616	2.4512	2.4538	66.2	–
1 0 6	48.805	1.8645	1.864	21.2	15.3
1 1 0	55.487	1.6545	1.6545	15.5	20.3
2 0 1	65.591	1.4221	1.4266	11.3	0.64
2 0 3	68.261	1.3729	1.3759	37	27.5
2 0 6	76.554	1.2435	1.2376	8.6	13.1
1 1 8	77.013	1.2372	1.2309	8.3	0.08
0 0 12	77.775	1.2269	1.2269	9.7	9.1

Table A.2

Summary of XRD results for  $\text{Ti}_2\text{InC}$ . The calculated  $d$ s are based on  $c$  and  $a$  values of 14.077 Å and 3.31344 Å, respectively

$h k l$	$2\theta$ , measured	Observed $d$ , (Å)	Calculated $d$ , (Å)	$I/I_{\text{max}}$ measured	$I/I_{\text{max}}$ calculated [11]
0 0 2	12.546	7.0410	7.0386	14.4	20.3
0 0 4	25.276	3.5207	3.5193	14.5	11.9
1 0 0	32.955	2.7158	2.7145	19	20.3
1 0 1	33.602	2.6650	2.6654	6.7	18
1 0 2	35.423	2.5320	2.5326	3.5	8.4
1 0 3	38.3	2.3481	2.3496	100	100
1 0 5	46.441	1.9538	1.9541	3.8	6.9
1 0 7	56.946	1.6158	1.6158	3	6.1
1 1 0	58.879	1.5672	1.5672	8.8	19.6
1 1 2	60.411	1.5311	1.5297	1	3.4
1 1 4	65.213	1.4295	1.4316	1.9	4.6
1 1 6	72.491	1.3029	1.3032	23.9	17.7
0 0 12	82.088	1.1731	1.1731	6	–

Table A.3

Summary of XRD results for (Ti,Hf)<sub>2</sub>InC. The calculated *d*s are based on *c* and *a* values of 14.429 Å and 3.221 Å, respectively

<i>h k l</i>	<i>2θ</i> , measured	Observed <i>d</i> , (Å)	Calculated <i>d</i> , (Å)	<i>I</i> / <i>I</i> <sub>max</sub> measured
0 0 4	24.651	3.60857	3.6072	8.9
1 0 0	32.053	2.79012	2.7892	18.2
1 0 3	37.268	2.41081	2.4128	100
1 0 6	50.033	1.82157	1.8213	13.8
1 1 0	57.155	1.61034	1.61034	16.6
0 2 0	67.344	1.38933	1.3946	17
0 2 3	70.263	1.33859	1.3394	23.8
0 0 12	79.678	1.2024	1.2024	4.4

phases, the film was assumed to be In. To test this hypothesis, a Ti<sub>2</sub>InC sample was placed in vacuum and held at 900 °C for ~2 h, after which its surface was characterized. The XRD patterns (not shown) clearly showed the emergence of peaks corresponding to TiC<sub>x</sub>. SEM of the same surface (Fig. 2d) indicated that a complete restructuring of the surface occurs. When taken together with a loss in weight, it is clear that under vacuum and at temperatures around ~1000 K, the In-containing samples lost In most probably according to:



Furthermore, if the reasonable assumption is made that this reaction is endothermic, the decrease in *c<sub>p</sub>* observed for the Ti<sub>2</sub>InC sample (Fig. 5) can be accounted for. Given that the MAX phases do not melt congruently, but dissociate peritectically into the A-group element and the MX<sub>x</sub> phases, the behavior of In in these ternaries is not too surprising.

### Acknowledgements

We would like to thank Prof. F. Sommer (MPI Metallforschung, Stuttgart, Germany), for carrying out the heat capacity measurements and Mr. A. Ganguly for the lattice parameter measurements. This work was partially funded by the Division of Materials Research of the National Science Foundation (DMR, 0072067). The support of Prof. M. Ruehle and the Humboldt and Max Planck Foundations to one of the authors (MB) during his sabbatical leave in Germany is also gratefully acknowledged.

### Appendix A

Tables A.1–A.3 show summaries of the XRD results.

### References

- [1] M.W. Barsoum, Prog. Solid State Chem. 28 (2000) 201–281.
- [2] M.W. Barsoum, T. El-Raghy, J. Am. Ceram. Soc. 79 (7) (1996) 1953–1956.
- [3] M.W. Barsoum, D. Brodtkin, T. El-Raghy, Scripta Metall. Mater. 36 (1997) 535–541.
- [4] T. El-Raghy, A. Zavaliangos, M.W. Barsoum, S. Kalidini, J. Am. Ceram. Soc. 80 (1997) 513–516.
- [5] M.W. Barsoum, T. El-Raghy, Metall. Mater. Trans. 30A (1999) 363–369.
- [6] M.W. Barsoum, L. Farber, T. El-Raghy, Metall. Mater. Trans. 30A (1999) 1727–1738.
- [7] M.W. Barsoum, H.-I. Yoo, I.K. Polushina, V.Yu. Rud', Yu.V. Rud', T. El-Raghy, Phys. Rev. B 52 (2000) 10194–10199.
- [8] M.W. Barsoum, T. El-Raghy, C.J. Rawn, W.D. Porter, H. Wang, A. Payzant, C. Hubbard, J. Phys. Chem. Solids 60 (1999) 429–439.
- [9] M.W. Barsoum, C.J. Rawn, T. El-Raghy, A. Procopio, W.D. Porter, H. Wang, C. Hubbard, J. Appl. Phys. 87 (2000) 8407–8414.
- [10] M.W. Barsoum, T. El-Raghy, W.D. Porter, H. Wang, J.C. Ho, S. Chakraborty, J. Appl. Phys. 88 (2000) 6316.
- [11] H.-I. Yoo, M.W. Barsoum, T. El-Raghy, Nature 407 (2000) 581–582.
- [12] M.W. Barsoum, I. Salama, T. El-Raghy, J. Golczewski, W.D. Porter, H. Wang, H. Seifert, F. Aldinger, submitted.
- [13] M.W. Barsoum, M. Ali, T. El-Raghy, Metall. Mater. Trans. 31A (2000) 1857–1865.
- [14] T. El-Raghy, S. Chakraborty, M.W. Barsoum, J. Eur. Ceram. Soc. 20 (2000) 2619–2625.
- [15] A. Crossley, E.H. Kisi, J.W.B. Summers, S. Myhra, J. Phys. D: Appl. Phys. 32 (1999) 632.
- [16] W. Jeitschko, H. Nowotny, F. Benesovsky, Monatsh. Chem. 94 (1963) 1201.
- [17] H. Pierson, Handbook of Refractory Carbides and Nitrides, Noyes, Westwood, NJ, 1996.